

## High power quality maximum power point tracking-based islanding detection method for grid-connected photovoltaic systems

Bakhshi-Jafarabadi, Reza; Sadeh, Javad; Rakhshani, E.; Popov, M.

**DOI**

[10.1016/j.ijepes.2021.107103](https://doi.org/10.1016/j.ijepes.2021.107103)

**Publication date**

2021

**Document Version**

Final published version

**Published in**

International Journal of Electrical Power & Energy Systems

**Citation (APA)**

Bakhshi-Jafarabadi, R., Sadeh, J., Rakhshani, E., & Popov, M. (2021). High power quality maximum power point tracking-based islanding detection method for grid-connected photovoltaic systems. *International Journal of Electrical Power & Energy Systems*, 131, Article 107103. <https://doi.org/10.1016/j.ijepes.2021.107103>

**Important note**

To cite this publication, please use the final published version (if applicable). Please check the document version above.

**Copyright**

Other than for strictly personal use, it is not permitted to download, forward or distribute the text or part of it, without the consent of the author(s) and/or copyright holder(s), unless the work is under an open content license such as Creative Commons.

**Takedown policy**

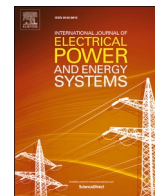
Please contact us and provide details if you believe this document breaches copyrights. We will remove access to the work immediately and investigate your claim.

***Green Open Access added to TU Delft Institutional Repository***

***'You share, we take care!' - Taverne project***

**<https://www.openaccess.nl/en/you-share-we-take-care>**

Otherwise as indicated in the copyright section: the publisher is the copyright holder of this work and the author uses the Dutch legislation to make this work public.



# High power quality maximum power point tracking-based islanding detection method for grid-connected photovoltaic systems

Reza Bakhshi-Jafarabadi <sup>a</sup>, Javad Sadeh <sup>a,\*</sup>, Elyas Rakhshani <sup>b</sup>, Marjan Popov <sup>b</sup>

<sup>a</sup> Department of Electrical Engineering, Ferdowsi University of Mashhad, Mashhad, Iran

<sup>b</sup> Faculty of EEMCS, Delft University of Technology, Mekelweg 4, 2628CD Delft, the Netherlands

## ARTICLE INFO

### Keywords:

Grid-connected photovoltaic system (GCPVS)  
Islanding detection  
Efficiency  
Maximum power point tracking (MPPT)  
Power quality (PQ)  
Non-detection zone (NDZ)

## ABSTRACT

Islanding is a condition when distributed generators (DGs) are disconnected electrically from the upstream network. This unwanted situation should be detected effectively to ensure the safety of the maintenance staffs and power quality (PQ) requirements. This paper presents a new high PQ maximum power point tracking (MPPT)-based methodology for detecting the islanding operating mode of grid-connected photovoltaic systems (GCPVSSs). In the recommended two-level scheme, a disturbance is injected into the MPPT algorithm under suspicious conditions, recognized by a passive criterion. This disturbance declines the DG active power output remarkably, drifting the output voltage beyond the minimum standard set in islanding state while its impact is negligible at the network presence. The effectiveness of the proposed technique has been evaluated through several hardware-in-the-loop simulations for a case study system, containing two power plant GCPVSSs equipped with a pair of multi-functional relays. The results highlight precise islanding classification within 137 ms with the small non-detection zone. Moreover, the results of PQ analyses indicate acceptable total demand distortion and harmonic spectra of the output current in compliance with the existing standards under various DG power penetrations. Since the presented scheme diminishes the active power output in case of suspicious islanding events, its influence on GCPVS efficiency has been studied as well. The outputs underline that the efficiency drops by 0.52% whilst the disturbance is stimulated every minute of the time. It is finally concluded that the proposed technique provides a reliable islanding classification as well as insignificant degradation of PQ and efficiency.

## 1. Introduction

Clean energy production, noise-free operation, low maintenance, and peak shaving during summer noon are some reasons to motivate grid-connected photovoltaic systems (GCPVSSs) around the world [1].

Despite the aforementioned advantages, just as other distributed generators (DGs), the connection of GCPVSSs to the network poses a few technical challenges such as islanding. Islanding occurs when a part of the utility including one or multiple DGs get disconnected from the upstream network but feeds solely the local loads. In this undesirable situation [2,3]:

- The frequency and the voltage of the isolated area may deviate from the standard range, damaging sensitive equipment.
- The safety of the maintenance crew who suppose the islanded area is de-energized is jeopardized.

- The transient overvoltage/overcurrent of the out-of-phase reclosing may damage the transformer, DG(s), and local load(s).

Therefore, this condition must be detected effectively to avoid these hazards. In this regard, IEC 61,727 and IEEE std 1547–2003 determine 2 s as the maximum permissible time for islanding protection [4,5].

### 1.1. Literature review

Several islanding detection methods (IDMs) categorized generally into the remote [6,7] and local groups, including passive [8–17], active [18–25], and hybrid [26–28] have been reported in the literature. Remote schemes are based on a channel between the upstream sub-station and DG(s). When the broadcast signal is not received by the receiver embedded at the DG end, an islanding state is identified [6,7]. These methods distinguish islanding and non-islanding incidents reliably without reducing the power quality (PQ). However, the high

\* Corresponding author.

E-mail address: [sadeh@um.ac.ir](mailto:sadeh@um.ac.ir) (J. Sadeh).

<https://doi.org/10.1016/j.ijepes.2021.107103>

Received 21 September 2020; Received in revised form 16 February 2021; Accepted 11 April 2021

Available online 30 April 2021

0142-0615/© 2021 Elsevier Ltd. All rights reserved.

Nomenclature			
<b>Variables</b>		$V_{PCC}$	PCC voltage
$\Delta P$	active power mismatch	$V_{PV,ref}$	PV array reference voltage
$\Delta Q$	reactive power mismatch	$V_T$	voltage threshold
$\alpha$	ratio of PV disturbance voltage to MPP	$V_{OC}$	PV array open-circuit voltage
$\beta$	ratio of PV open-circuit voltage to MPP	$Z_r$	rotor impedance
$ \Delta V_{PCC} $	absolute PCC voltage deviation	$Z_s$	stator impedance
$E_L$	GCPVS energy loss	<b>Acronyms</b>	
$I_{SC}$	PV array short-circuit current	AFD	active frequency drift
$I_{MPP}$	PV array MPP current	CB	circuit breaker
$I_{NEW}$	new PV array current	DG	distributed generator
$X_m$	magnetizing inductance	FDZ	false detection zone
$P_{DIS}$	active power disturbance	GCPVS	grid-connected photovoltaic system
$P_{DG}$	DG active power output	GMPP	global maximum power point
$P_{NEW}$	new PV array power	HiL	hardware-in-the-loop
$P_{MPP}$	PV array MPP power	IDM	islanding detection method
$P_{PV}$	PV array power	LMPP	local maximum power point
$Q_f$	load quality factor	MPP	maximum power point
$R_S$	PV array series resistance model	MPPT	maximum power point tracking
$t_D$	duration of disturbance injection	NDZ	non-detection zone
$t_S$	disturbance starting time	PCC	point of common coupling
$t_T$	disturbance total duration	PQ	power quality
$TDD_i$	TDD of output current	RTDS	real-time digital simulator
$THD_i$	THD of output current	SFS	sandia frequency shift
$V_{DIS}$	disturbance voltage	STC	standard test condition
$V_{MPP}$	PV array MPP voltage	TDD	total demand distortion
$V_{NEW}$	new PV array voltage	THD	total harmonic distortion
$V_{pr}$	pre-islanding PCC voltage	UV	undervoltage
$V_{po}$	post-islanding PCC voltage	VPF	voltage positive feedback
$V'_{po}$	PCC voltage after disturbance injection	VSI	voltage source inverter

burden cost is the main drawback of such IDMs, especially for small-scale microgrids.

In case of local IDMs, a criterion of the point of common coupling (PCC) is monitored continuously. In passive techniques, islanding is found whilst the local yardstick deviates the preset threshold(s) regarding the cut of transferred power from/into the utility, e.g. rate of change of equivalent resistance at PCC [8]. Xie, et al. showed that the mentioned index raises sharply when the grid is lost, distinguishing the islanding operation mode except for the narrow  $\pm 1\%$  range of relative power mismatches. Nikolovski, et al. adopted the rate of change of reactive power of biomass unit as an islanding detection criterion [9]. The required reactive power is provided by the utility in the grid-tied mode to ensure unity power factor operation of the DG. During the islanding, however, the imported reactive power is cut and the aforementioned variable surpasses a preset threshold within 100 ms. Generally speaking, the passive methods are realized simply and have no adverse impact on PQ in the normal operating conditions. Nevertheless, these IDMs suffer a large non-detection zone (NDZ), i.e. the islanding scenarios without successful detection. The threshold(s) selection is another challenge, fulfilled as a tradeoff between minimum NDZ and false tripping [8–12].

Recently, mathematical tools are applied to find the islanding mode through a pattern recognition algorithm or a frequency-based criterion [13–17]. Although these passive algorithms discriminate islanding and non-islanding situations precisely, they need a high burden data in training and classification processes. The settings, which are defined through extensive islanding and non-islanding tests, are heavily relied upon the studied system as well. Thus, these scenarios should be repeated in the training process for a new DG/network to regenerate the settings.

In active plans, a controlled disturbance is involved in the DG

controller to accelerate/signify the deviation of a local yardstick, mitigating the NDZ and shortening the detection time. However, the quality of the DG active power output may be degraded due to the amplification of the current harmonics. The disturbance amplitude and the time duration have been thereby limited to the upper bounds to satisfy the PQ requirements [18–25,29]. For instance, the injection of the reactive power has been presented in active frequency drift (AFD) to shift the frequency out of the standard limits [18]. Although the amount of reactive power disturbance can be assigned larger to achieve a smaller NDZ, Lopes and Sun showed that it should be limited within the  $[-0.95\%, 4.11\%]$  range to keep the total harmonic distortion (THD) of the output current ( $THD_i$ ) below 5%. Yafouni, et al. developed an adaptive disturbance in sandia frequency shift (SFS) algorithm to accomplish the same NDZ of AFD with 30% less  $THD_i$  [19]. A larger disturbance can be injected to lessen NDZ with acceptable PQ accordingly. In impedance measurement technique, the insertion of a high-frequency current to a single DG of multi-DGs case has been suggested by Reigosa, et al. [20]. By this, acceptable PQ is guaranteed for all power penetrations while islanding is categorized through the equipped DG. For voltage positive feedback (VPF), a PCC voltage disturbance is inserted into the  $d$ -axis reference current to destabilize the output voltage during islanding [21]. This aim is achieved by changing the DG active power output ( $P_{DG}$ ), i.e. current amplitude after the island formation. The presented analyses by Samui and Samantaray underlined an outstanding performance of VPF even in the presence of the static load. These authors claimed that the conventional VPF fails to recognize islanding mode of a GCPVS with the surplus active power [22]. In such cases, the  $P_{DG}$  cannot be raised due to the lack of input power in a given meteorological condition. Consequently, an absolute voltage negative feedback has been recommended to decline the active power output in all possible scenarios. According to the presented outputs, the NDZ of

the VPF is eliminated successfully by the modified algorithm and islanding is categorized in all states within 250 ms.

The combination of the passive and active IDMs is the basis of hybrid techniques [26–28]. In such schemes, the active disturbance is triggered under suspicious cases, detected by a passive criterion. As a result, the PQ remains unchanged during the normal operating point while islanding events with small power mismatch can be found by the active disturbance. Rostami, et al. exploited the rate of change of PCC voltage to identify the suspicious islanding situations [26]. A parallel inductance is then connected at the PCC to push this variable out of the preset range. The simulation results endorse successful performance of the presented two-level algorithm in all critical scenarios within 300 ms. However, similar to the active and passive IDMs, the threshold selection is a major challenge of such hybrid IDMs to acquire the minimum NDZ and false operation.

It can be concluded from the literature that the presentation of a new high PQ IDM is of interest. The proposed technique should classify islanding situations quickly without nuisance tripping in non-islanding switching transients.

### 1.2. Contribution and paper structure

This paper aims to present a new two-level maximum power point (MPP) tracking (MPPT)-based IDM for the GCPVS-based microgrid. The proposed technique has been structured in a way that a disturbance is injected into the MPPT algorithm under suspicious islanding events. By this means, the  $P_{DG}$  diminishes sharply for shifting the PCC voltage below the minimum standard set. The provided technique presents various advantages, including:

- Accurate classification with small NDZ in at most 137 ms.
- Simple and inexpensive structure.
- Employing low burden data, i.e. RMS samples of the PCC voltage.
- Automatic MPP restoration to contribute fully in the power supply of the autonomous microgrid.
- Insignificant influence on the output PQ.

The rest of the paper is organized as follows. The proposed two-level IDM and the selection criterion of the settings are described in Section 2. The case study system is initially introduced in Section 3, and the functionality of the presented scheme is then appraised through several hardware-in-the-loop (HiL) tests. In Section 4, the effect of the recommended IDM on the PQ and efficiency of the GCPVS is evaluated. The proposed algorithm is then compared to a few existing IDMs from the paramount islanding detection features in Section 5. This section also discusses the obtained results and main achievements of the current work. Finally, the concluding remarks are elaborated in Section 6.

## 2. Two-level maximum power point tracking-based algorithm

In this section, the presented two-level methodology and its thresholds selection criterion have been described. In the first level of the current scheme, the voltage threshold is determined in the term of NDZ. The disturbance voltage of the second level should be also defined in a way that the PCC voltage crosses the minimum standard edge in all islanding scenarios.

### 2.1. Methodology description

During the normal operating mode, the load power is supported by both the DG and the grid as depicted in Fig. 1. In this condition, the PCC voltage can be expressed as follows:

$$P_L = P_{DG} - \Delta P = \frac{V_{pr}^2}{R} \quad (1)$$

where,  $R$  is defined as the resistive part of the parallel RLC branch of

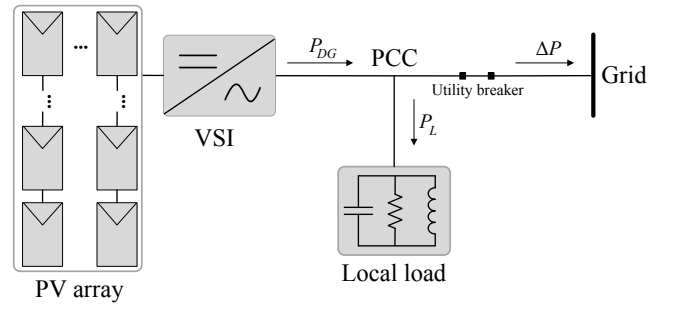


Fig. 1. Connection of GCPVS to the network.

the local load model, according to IEEE std 929–2000 [30]. Furthermore,  $V_{pr}$ ,  $\Delta P$ , and  $P_L$  represent pre-islanding PCC voltage, active power mismatch fed into/received from the grid, and load active power, respectively. After island formation, the grid power is cut and the post-islanding PCC voltage ( $V_{po}$ ) can be quantified as follows:

$$P_L = P_{DG} = \frac{V_{po}^2}{R} \quad (2)$$

By combining Eqs. (1) and (2), the  $V_{po}$  can be expressed in the terms of pre-islanding PCC voltage and real power mismatch:

$$V_{po} = V_{pr} \sqrt{\frac{1}{1 - \frac{\Delta P}{P_{DG}}}} \quad (3)$$

According to Eq. (3), the  $V_{po}$  leaves the standard voltage [88%–110%] range for [–29.13%, 17.35%] of the relative active power mismatches ( $\Delta P/P_{DG}$ ) under  $V_{pr} = 100\%$ . The employment of an effective IDM is therefore mandatory to classify islanding under such critical circumstances.

Apart from this, there are two independent controllers in a voltage source inverter (VSI) of a GCPVS. The internal control loop (DC/AC converter) balances the input and output powers and synchronizes the output current to the PCC voltage ( $V_{PCC}$ ) while the MPPT algorithm is accomplished in the external control

loop (DC/DC converter) [31]. In a search-based MPPT technique, a disturbance is injected into the PV array reference voltage ( $V_{PV,ref}$ ) and its output power ( $P_{PV}$ ) is measured. A same/opposite disturbance is employed in the next time frame under the rise/fall of  $P_{PV}$  [32]. Therefore, the reference voltage is ultimately set around the MPP voltage ( $V_{MPP}$ ) as illustrated in Fig. 2. In this figure, short-circuit current, MPP current, MPP power, and open-circuit voltage are denoted by  $I_{SC}$ ,  $I_{MPP}$ ,  $P_{MPP}$ , and  $V_{OC}$ , respectively.

As shown in the flowchart of the two-level IDM in Fig. 3, a

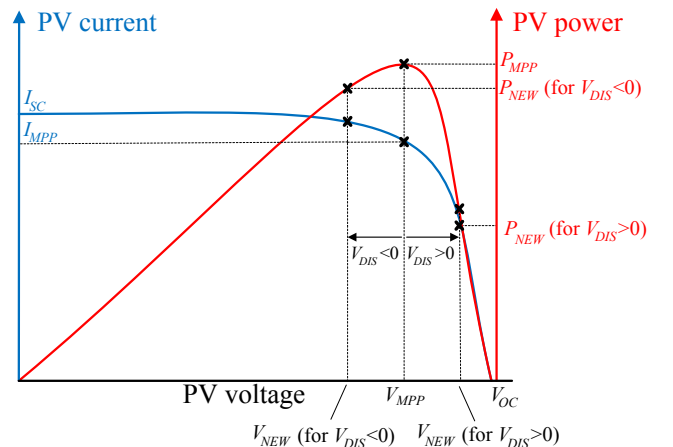


Fig. 2. MPPT realization in a GCPVS.

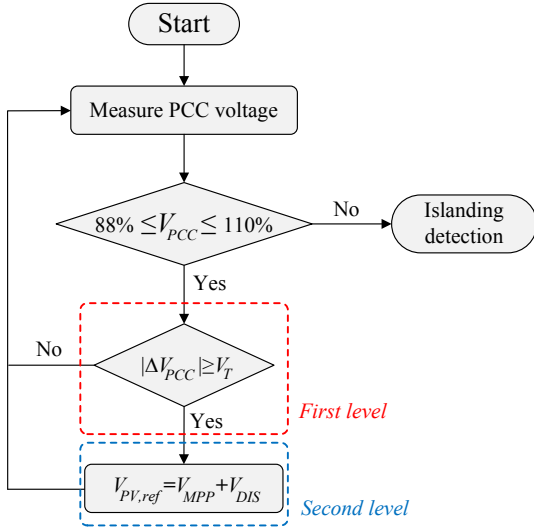


Fig. 3. Flowchart of the proposed two-level MPPT-based IDM.

disturbance voltage ( $V_{DIS}$ ) is inserted into the MPPT algorithm under suspicious islanding circumstances. These events are identified in the first level whilst the absolute PCC voltage deviation ( $|\Delta V_{PCC}|$ ) exceeds a voltage threshold ( $V_T$ ). Subsequently, a disturbance voltage is injected into  $V_{PV,ref}$  in the second level as in Eq. (4) to deviate PV operating point from MPP, reducing the DG active power output notably:

$$V_{PV,ref} = V_{MPP} + V_{DIS} \quad (4)$$

The PV operating point moves to a *new* condition labeled as  $I_{NEW}$ ,  $V_{NEW}$ , and  $P_{NEW}$  for current, voltage, and power, respectively. According to Fig. 2, the  $P_{PV}$  declines by the imposed disturbance for both situations ( $V_{DIS} > 0$  and  $V_{DIS} < 0$ ); however, the power drops greater in the right-hand side of MPP for a given  $V_{DIS}$ . Moreover, the disturbance which is triggered for a short-time duration, e.g. 0.2 s, has switched off for 2 s to restore MPP after islanding classification. By this means, the GCPVS generates its maximum available power in the standalone microgrid as conveyed in the next section.

When the grid is present, the PCC voltage is strictly governed by the utility and the impact of the active power output drop is negligible. Conversely, this active power fall shifts the PCC voltage to a new level in islanding mode ( $V'_{po}$ ), defined as follows:

$$V'_{po} = V_{po} \sqrt{\frac{1}{1 - \frac{P_{DIS}}{P_{DG}}}} \quad (5)$$

where,  $P_{DIS}$  is the real power output reduction after the disturbance injection. It is worth mentioning that the recent expression is derived by using Eq. (3) during islanding mode, before and after inserting the proposed disturbance. In order to distinguish the islanding operating mode, the  $V'_{po}$  should be shifted beyond the minimum voltage set to stimulate the undervoltage (UV) relay. Fig. 4 depicts the required  $P_{DIS}$  to ride a PCC voltage inside the [88%, 110%] range below 88%. It is seen that the required  $P_{DIS}$  to achieve this goal is 56.25% for the worst scenario, i.e.  $V_{po} = 110\%$  to  $V'_{po} = 88\%$  transition. The  $V_{DIS}$  should be determined so that the  $P_{DIS}/P_{DG}$  would be smaller than  $-56.25\%$  in all situations accordingly. The selection criterion of this variable and voltage threshold is described in the next subsection.

### 2.2. Thresholds selection criterion

Voltage threshold and disturbance voltage are two settings of the recommended algorithm. Suspicious islanding cases have been identified by comparing  $|\Delta V_{PCC}|$  to the voltage threshold. The NDZ would be larger under a greater  $V_T$  selection, i.e. the disturbance has not been

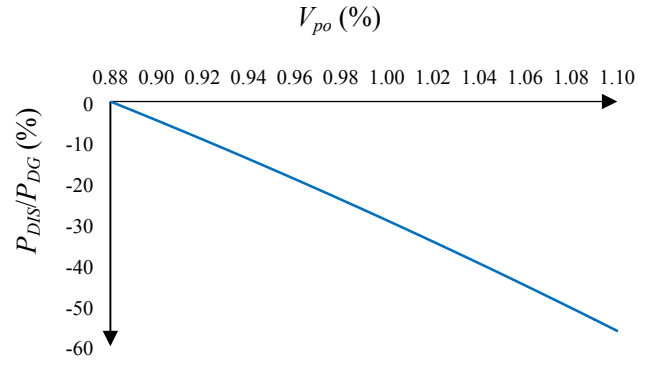


Fig. 4. Disturbance active power to shift output voltage beyond the minimum standard set.

activated in more islanding events. Contrary to this, the undesirable disturbance injection would increase under non-islanding switching transients such as motor/capacitor bank switching; hence, the efficiency degradation climbs for a smaller  $V_T$ . Since the disturbance time duration is too short, the  $V_T$  is defined in the term of NDZ in this paper. In this regard, the NDZ of a given  $V_T$  includes the  $\Delta P/P_{DG}$  sets in Eq. (3) with  $|\Delta V_{PCC}| < V_T$ , i.e. the proposed disturbance remains OFF. Fig. 5 illustrates the NDZ of the proposed IDM for several  $V_T$ s under  $V_{pr} = 100\%$ . The provided outputs confirm that the NDZ of the presented scheme is small, e.g.  $\pm 1\%$  for  $V_T = 0.5\%$ , especially in comparison with the commercial voltage relay with  $[-29.13\%, 17.35\%]$  NDZ.

Disturbance voltage is another setting that should be established accurately to drift  $V_{PCC}$  below the UV relay setting in the second level. This aim is accomplished when the  $P_{DIS}/P_{DG}$  would be less than  $-56.25\%$  as explained earlier. The PV array current vs. voltage on the right-hand side of MPP is considered in the uniform received radiation mode to quantify  $V_{DIS}$ . This slope is defined as a PV series resistance ( $R_S$ ) in the single-diode representation as shown in Fig. 6 [33]. According to  $R_S$ , the relation between MPP, *new*, and open-circuit operating points can be given by:

$$R_S^{-1} = \frac{I_{NEW} - I_{MPP}}{V_{NEW} - V_{MPP}} = \frac{-I_{MPP}}{V_{OC} - V_{MPP}} \quad (6)$$

Eq. (6) can be simplified as follows by assuming  $V_{NEW} = (1 + \alpha)V_{MPP}$  and  $V_{OC} = (1 + \beta)V_{MPP}$ , where  $\beta$  can be determined using the ratio of  $V_{OC}$  to  $V_{MPP}$  in the module datasheet. Furthermore,  $\alpha$  should be computed to establish  $V_{DIS}$ , i.e.  $V_{DIS} = \alpha V_{MPP}$ .

$$\frac{I_{NEW}}{I_{MPP}} = \frac{\beta - \alpha}{\beta} \quad (7)$$

After disturbance injection, the new PV module power can be given by:

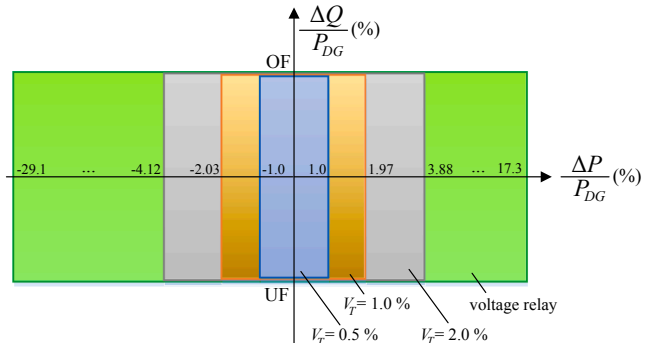


Fig. 5. NDZ of the proposed IDM in the term of voltage threshold.

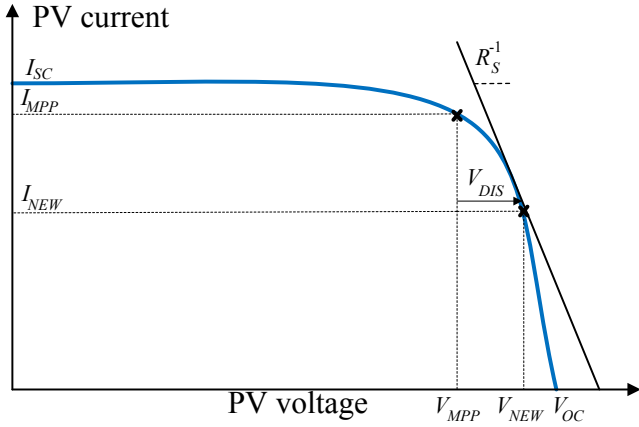


Fig. 6. Disturbance voltage selection in the second-level of the recommended technique.

$$P_{NEW} = V_{NEW} \times I_{NEW} = (1 + \alpha)V_{MPP} \times (1 - \alpha\beta^{-1})I_{MPP} \quad (8)$$

Finally, the relative active power drop ( $P_{DIS}/P_{DG}$ ) is deduced by neglecting the VSI's losses, i.e.  $P_{DG} = P_{MPP}$ :

$$\frac{P_{DIS}}{P_{DG}} = (\alpha - \alpha\beta^{-1} - \alpha^2\beta^{-1}) \quad (9)$$

This second-order equation can be solved to find  $\alpha$  for a specific  $\beta$  with  $P_{DIS}/P_{DG} = -56.25\%$ . Therefore, the disturbance voltage size can be quantified accurately to reduce PCC voltage for categorizing the islanding operation in all cases.

In this paper,  $V_T$  is assigned 0.5% to stimulate the disturbance voltage for all relative active power mismatches except a narrow  $\pm 1\%$  range. Besides,  $\beta$  of the employed PV module, introduced in the next subsection, is 25%; thus, Eq. (9) results in  $-90.53\%$  (not acceptable) and 15.5% (acceptable). The selection of 20% for  $\alpha$  ensures a successful shift of PCC voltage under UV set after disturbance activation in all islanding scenarios.

### 3. Islanding assessment

The authenticity of the proposed IDM has been examined through various HiL tests in this section. The information of the studied network with two large-scale GCPVSs is detailed in Fig. 7 and Table 1. In VSI of the GCPVSs, the perturb and observe MPPT algorithm is employed in the

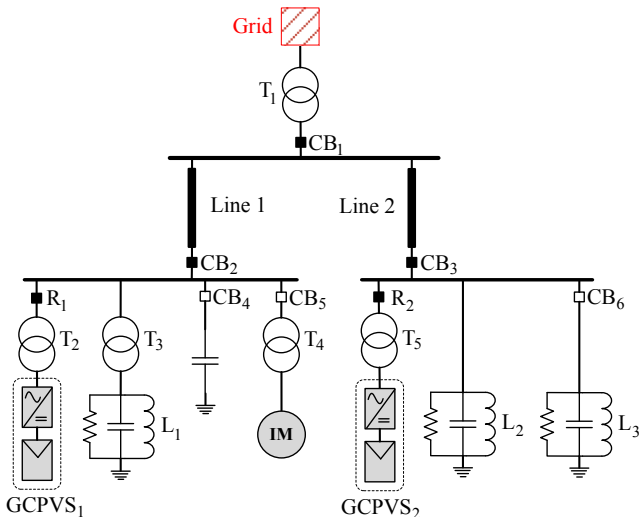


Fig. 7. Case study system for islanding and non-islanding assessment.

Table 1  
Detailed characteristics of the studied system.

Equipment	Description
Grid	400 kV, 50 Hz, 1000 MVA
Local load	L <sub>1</sub> : 0.4 kV, R = 0.16 Ω; L <sub>2</sub> : 13.2 kV, R = 58.08 Ω; L <sub>3</sub> : 13.2 kV, Z = 58.08 ± j58.08 Ω
Line	Line 1: 5 km, Z <sup>1</sup> = 0.17 + j1.56 Ω, Z <sup>0</sup> = 1.16 + j4.55 Ω; Line 2: 15 km, Z <sup>1</sup> = 0.44 + j4.63 Ω, Z <sup>0</sup> = 3.49 + j13.65 Ω
Transformer	T <sub>1</sub> : 4.8 MVA, 400/13.2 kV, YΔ11; T <sub>2</sub> and T <sub>3</sub> : 1.2 MVA, 13.2/0.4 kV, YΔ11; T <sub>4</sub> : 1.0 MVA, 13.2/0.4 kV, YΔ11; T <sub>5</sub> : 3.6 MVA, 13.2/0.4 kV, YΔ11
GCPVS	DG <sub>1</sub> : 1 MW, DG <sub>2</sub> : 3 MW (PV module: V <sub>MPP</sub> = 37.0 V, I <sub>MPP</sub> = 8.25 A, V <sub>OC</sub> = 46.3 V, I <sub>SC</sub> = 8.87 A)
Induction motor	500–1000 HP, 0.4 kV, Z <sub>s</sub> = 0.04 + j0.09p.u., Z <sub>r</sub> = 0.05 + j0.07p.u., X <sub>m</sub> = 2.97p.u.

DC stage while the AC stage exploits a pulse width modulation technique.

The case study system has been simulated in RSCAD using four real-time digital simulator (RTDS) PB5 cards while two multi-functional physical digital relays are equipped at the DGs' ends (R<sub>1</sub> and R<sub>2</sub> in Fig. 7). Analog and digital communication signals are sent to these relays through two amplifiers and a gigabit transceiver analogue card (Fig. 8). The voltage of these relays, set with IEEE std 1547–2003 [5] is applied to compute  $V_{PCC}$  and  $|\Delta V_{PCC}|$  in the detection procedure. The PQ indices, including total demand distortion (TDD) of the output current (TDD<sub>I</sub>) and harmonic spectra are also estimated through the relays' current.

The islanding analyses include different active/reactive power mismatches in standard test condition (STC) (cases 1–7) and non-STC (cases 8–13), various load quality factors (cases 14–18), and multi-DG scenarios (cases 19–22). Several non-islanding disturbances, including motor starting, capacitor bank switching, and sudden load change are simulated in real-time (cases 23–30) as well. All these cases, tabulated in Table 2, are yielded by opening/closing circuit breakers (CBs) at  $t = 1$  s.

#### 3.1. Active and reactive power mismatches

Referring to Eq. (3), the active power imbalance plays a vital role in the PCC voltage variation after island formation. The islanding standards also emphasize conducting the tests for different relative reactive power mismatches ( $\Delta Q/P_{DG}$ ) inside the  $\pm 5\%$  range [4,5]. The initial studies have been thereby carried out for different  $\Delta P$  and  $\Delta Q$  sets. All tests are performed in the STC where the received insolation and the cell temperature are 1000 W/m<sup>2</sup> and 25 °C, respectively. In Fig. 9 (a), the results of case 1, including the PV reference voltage, PCC voltage, and active power output are illustrated. The variation of the output voltage for a few case studies is presented in Fig. 9 (b) as well.

It is readily observed from Fig. 9 that the absolute PCC voltage exceeds  $V_T$  after islanding inception and a disturbance is injected into the  $V_{PV,ref}$  subsequently. Since the PV array losses MPP performance by means of the imposed disturbance,  $P_{DG}$  diminishes by around 60%. This active power drop leads to a sharp PCC voltage fall, under the UV protection setting. Therefore, the presented methodology categorizes islanding in all states within 136 ms except in a well-balanced island in where the disturbance has not been stimulated due to the small voltage fluctuation ( $|\Delta V_{PCC}| < V_T$ ). These results match with the estimated NDZ in Section 2.2 for  $V_T = 0.5\%$  which includes  $\pm 1\%$  of the relative active power mismatches. Furthermore, the MPP has been restored by the MPPT algorithm after disturbance clearance (within 500 ms) and  $P_{DG}$  has

re-established at its maximum level. Hence, the GCPVS can produce its full active power in the autonomous microgrid to support the critical loads and sustain the frequency and voltage stability.

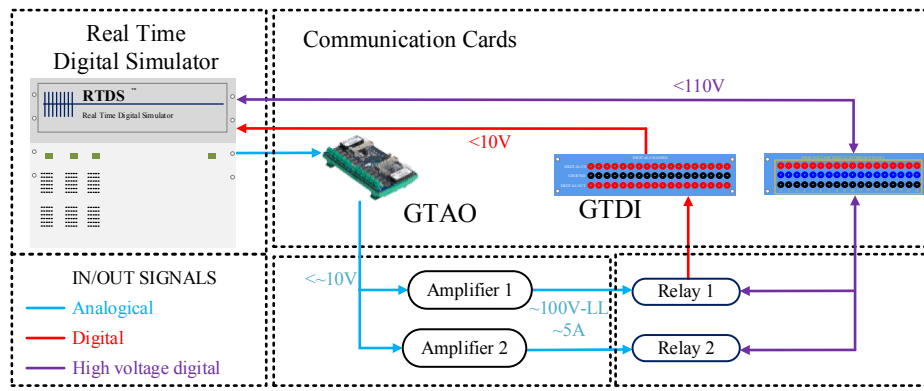


Fig. 8. Case study system realization in real-time simulations.

### 3.2. Non-standard test condition

The performance of renewable energy resources relies heavily on the climate condition. In addition to the STC, the proposed two-level IDM should identify islanding states in other meteorological situations accordingly. As tabulated in Table 2, non-STC is yielded by reducing the received solar radiation to  $750 \text{ W/m}^2$  and  $500 \text{ W/m}^2$  and regenerating the local load sets to simulate various active and reactive power mismatches. According to the PCC voltage waveform of cases 8 and 13, displayed in Fig. 10, the proposed disturbance has been triggered and  $P_{DG}$  reduces notably in all scenarios regarding the active/reactive power mismatches. The  $V_{PCC}$  is thereby shifted to the lower margin within 135 ms. Thus, the performance of the two-level scheme is secure in all operating conditions.

### 3.3. Load quality factor

The assessment has been developed for different load quality factors ( $Q_f$ s) as emphasized in IEEE std 1547–2003 [5]. The local load is tuned in cases 14–18 to simulate  $Q_f$  between 0.5 and 8.0 with a + 5% active power mismatch. What stands from the illustrated outputs in Fig. 11 and Table 2, the PCC voltage is shifted effectively to the lower bound owing to the active power mismatch created by the imposed disturbance. Therefore, the islanding mode has been recognized by the UV protection in all events irrespective of the  $Q_f$  set.

### 3.4. Multi-distributed generator

In a few active IDMs, the connection of multi-DG may result in interference performance of the injected disturbance and nuisance tripping [20,25]. The study has been extended to the multi-DG case in scenarios 13–16 to this end. The first and the second load are adjusted to simulate different power imbalances. The results of case 15, including  $V_{PCC}$  and  $P_{DG}$  of both GCPVSs, have been depicted, respectively in Fig. 12 (a) and (b), as an instance. In these figures, the variables of the first and second GCPVSs are denoted by “1” and “2” subscript. It can be inferred from the outputs that the proposed methodology declines the DGs’ active power output successfully during the 1.05–1.25 s time frame. Consequently, the output voltage plummets significantly so that the UV relay has been triggered. Moreover, the active power output of both GCPVSs is restored to MPP, settling the PCC voltages around the nominal level. As explained earlier, this facilitates the frequency and voltage recovery as well as supplying the critical load(s) of the standalone microgrid.

### 3.5. Non-islanding disturbances

The electrical power system is exposed to various non-islanding disturbances such as capacitor bank switching, induction motor

starting, and sudden load change. During these transient switching events, the PCC voltage may change in a way the proposed disturbance is triggered ( $|\Delta V_{PCC}| \geq V_T$ ). Hence, although the active power descent is inevitable in these circumstances, the PCC voltage should not leave the standard limits.

The effectiveness of the presented MPPT-based IDM has been investigated under several non-islanding incidents and the PCC voltage of a few scenarios is illustrated in Fig. 13. In these conditions, the size of active/reactive power change is chosen in a way that the imposed disturbance is fired. From the outputs, it is found that the reduced active power output has an eminently negligible influence on the output voltage since it is controlled fully by the electrical network. Therefore, the proposed two-level technique exhibits no false detection zone (FDZ) in such switching transients.

Despite promising outputs of islanding and non-islanding investigations, the proposed scheme should provide an acceptable PQ in all power penetrations. The paramount PQ indices affected by the presented IDM are measured in the next part. Since the recommended approach declines the active power output for islanding detection, efficiency degradation is also studied in the following HiL simulations.

## 4. Power quality evaluation

The effect of two-level MPPT-based IDM on the PQ of the output current has been investigated in this section. Although PQ includes various indices,  $TDD_I$  and harmonic spectra are highly affected by active and hybrid IDMs and therefore, considered in this study [18–21,24,29]. In the literature, efficiency has been rarely debated in the PQ analysis. Nevertheless, since the active power output drops during the suspicious islanding events, the study has been extended for GCPVS’s efficiency as well.

### 4.1. Total demand distortion and harmonic spectra

Total demand distortion of the DG current should be restricted to 5% for all operating conditions as postulated in IEEE std 1547–2003 and IEC 61,727 [4,5]. This parameter should be also computed regarding the GCPVS output current in a given meteorological condition. In this perspective, the disturbance voltage is triggered at  $t = 1 \text{ s}$  under four insolation levels and  $TDD_I$  at 1 MW GCPVS terminal has been measured.

The results in Fig. 14 indicate that  $TDD_I$  goes up during the disturbance injection, especially at the lower DG generation level. However, it is at most 2.42% which is less than the maximum permissible set. The maximum  $TDD_I$  at 500, 750, and  $1000 \text{ w/m}^2$  are also 1.45, 1.32, and 0.86%, respectively. These outputs imply the insignificant influence of the MPPT-based injection IDM on the PQ. These encouraging results are achieved since the inserted disturbance does not signify the current harmonics.

Despite  $TDD_I$ , the current harmonics of the GCPVS should be limited

**Table 2**  
Islanding and non-islanding scenarios and outputs.

Case No.	Case study	Details	Detection time (ms)
1	Active and reactive power mismatches in STC (Opening $CB_2$ at $t = 1$ s)	$\Delta P = 0.05$ MW, $\Delta Q = 0$	114
2		$\Delta P = -0.05$ MW, $\Delta Q = 0$	31
3		$\Delta P = 0$ , $\Delta Q = 0$	-
4		$\Delta P = 0.05$ MW, $\Delta Q = 0.05$ Mvar	37
5		$\Delta P = 0.05$ MW, $\Delta Q = -0.05$ Mvar	42
6		$\Delta P = -0.05$ MW, $\Delta Q = 0.05$ Mvar	40
7		$\Delta P = -0.05$ MW, $\Delta Q = -0.05$ Mvar	136
8	Active and reactive power mismatches in non-STC with $P_{DG} = 0.75$ MW (Opening $CB_2$ at $t = 1$ s)	$\Delta P = 0.037$ MW, $\Delta Q = 0.037$ Mvar	102
9		$\Delta P = 0.037$ MW, $\Delta Q = 0$ Mvar	135
10		$\Delta P = -0.037$ MW, $\Delta Q = -0.037$ Mvar	106
11	Active and reactive power mismatches in non-STC with $P_{DG} = 0.5$ MW (Opening $CB_2$ at $t = 1$ s)	$\Delta P = 0.025$ MW, $\Delta Q = 0.025$ Mvar	121
12		$\Delta P = 0.025$ MW, $\Delta Q = 0$ Mvar	131
13		$\Delta P = -0.025$ MW, $\Delta Q = -0.025$ Mvar	110
14	Load quality factor with $\Delta P = 0.05$ MW (Opening $CB_2$ at $t = 1$ s)	$Q_f = 0.5$	58
15		$Q_f = 1.0$	62
16		$Q_f = 2.5$	137
17		$Q_f = 4.0$	94
18	Multi DGs (Opening $CB_1$ at $t = 1$ s)	$Q_f = 8.0$	76
19		$\Delta P = 0.2$ MW, $\Delta Q = 0.2$ Mvar	46
20		$\Delta P = 0.2$ MW, $\Delta Q = -0.2$ Mvar	33
21	Capacitor switching ON/OFF (Opening/closing $CB_4$ at $t = 1$ s)	$\Delta P = -0.2$ MW, $\Delta Q = 0.2$ Mvar	35
22		$\Delta P = -0.2$ MW, $\Delta Q = -0.2$ Mvar	21
23		$\Delta Q = -0.5$ Mvar	-
24	Sudden load change (Closing $CB_6$ at $t = 1$ s)	$\Delta Q = -1.0$ Mvar	-
25		$\Delta Q = 0.5$ Mvar	-
26		$\Delta Q = 1.0$ Mvar	-
27	Induction motor starting (Closing $CB_5$ at $t = 1$ s)	$\Delta P = 3.0$ MW, $\Delta Q = 3.0$ Mvar	-
28		$\Delta P = 3.0$ MW, $\Delta Q = -3.0$ Mvar	-
29	Induction motor starting (Closing $CB_5$ at $t = 1$ s)	$\Delta P = 500$ HP	-
30		$\Delta P = 1000$ HP	-

to the predefined sets, illustrated in Fig. 15 [4,5]. The harmonic components have been measured during the active power output drop time frame ( $t = 1$  to  $1.4$  s) and the maximum recorded current harmonics up to the 9th, have been displayed in Fig. 15. The outputs reveal that while the odd harmonics are far away the standard margin, the even harmonics are near to it, e.g. 0.90%, 0.98%, and 0.90% for 2nd, 6th, and 8th harmonics, respectively. Nonetheless, all harmonics are within the standard range in the presence of the proposed IDM.

According to the presented results, it can be inferred that the PQ requirements of the GCPVS, equipped with the presented technique are met under various generation levels.

#### 4.2. Efficiency

The presented islanding detection algorithm reduces  $P_{DG}$  through

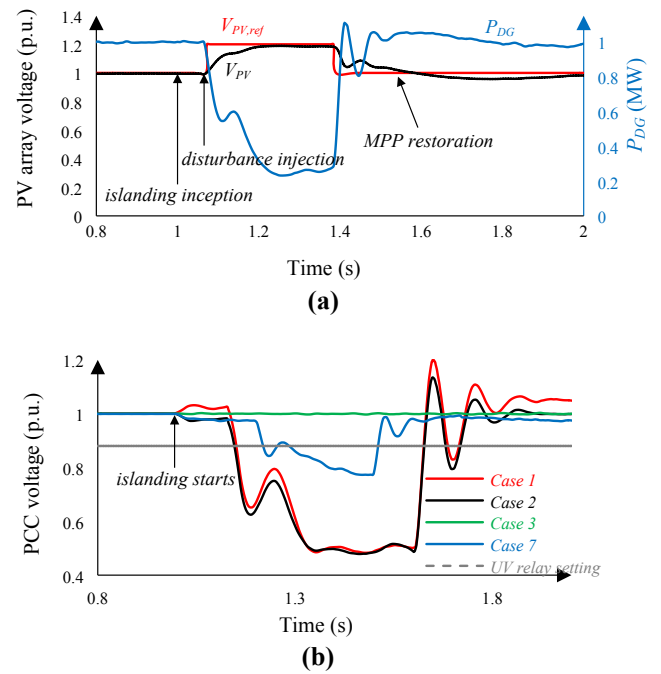


**Fig. 9.** Results of islanding simulation under various active and reactive power imbalances: (a) PV array voltage, PV array reference voltage, and GCPVS active power output (case 1); (b) PCC voltage.

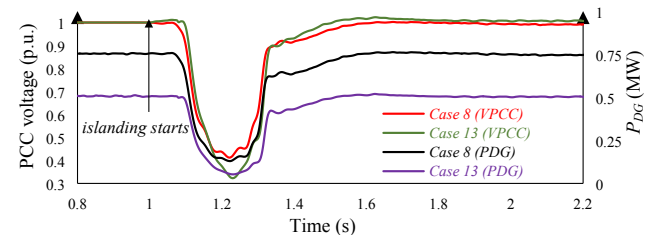


**Fig. 10.** Outputs of non-STC islanding scenarios.

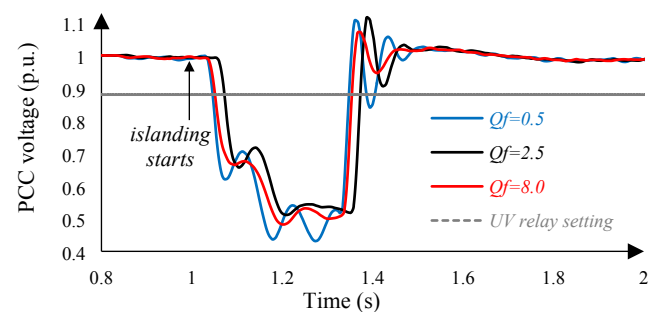


**Fig. 11.** Outputs of the islanding tests under various quality factors.

deviating PV array operating point from MPP as shown in Fig. 16. In order to determine the efficiency degradation, the GCPVS energy loss ( $E_L$ ) during the disturbance duration ( $t_D$ ), initiating at  $t_S$  can be computed as follows:

$$E_L = (P_{MPP} \times t_D) - \int_{t_S}^{t_S+t_D} P_{DG} dt \quad (9)$$

Furthermore, the GCPVS generated energy during the total disturbance time interval ( $t_T$ ) would be  $P_{MPP} \times t_T$  without imposing the

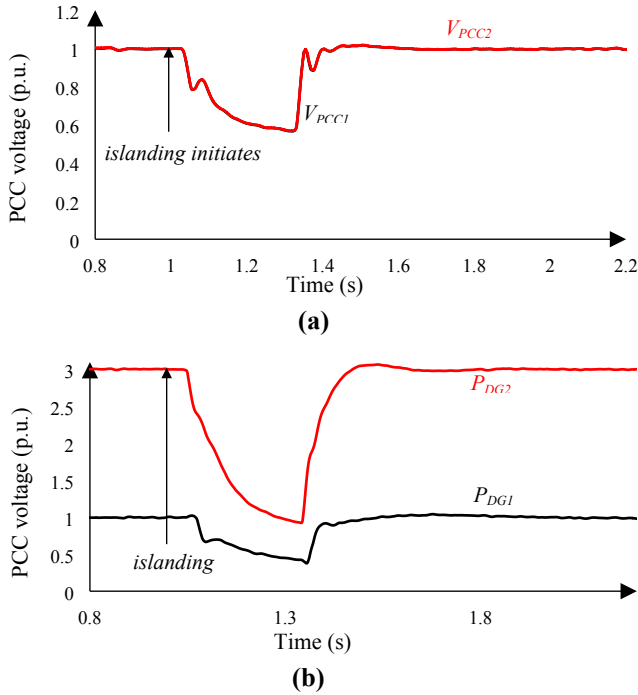


Fig. 12. Multi-DGs scenario with -5% relative active and reactive power mismatches: a) Active power, b) PCC voltage.

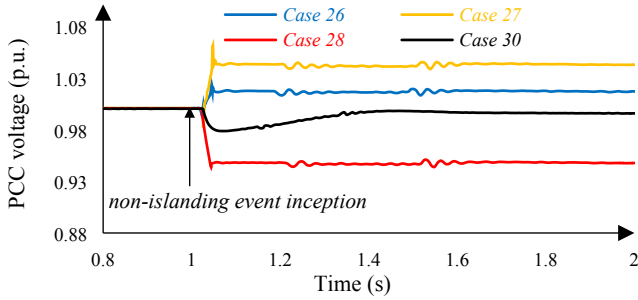


Fig. 13. Outputs of non-islanding HiL simulations.

proposed disturbance. Thus, the relative energy loss  $E_L/(P_{MPP} \times t_T)$  during the  $t_T$  time frame can be given by:

$$\frac{E_L}{P_{MPP} \times t_T} = \frac{(P_{MPP} \times t_D) - \int_{t_s}^{t_s+t_D} P_{DG} dt}{P_{MPP} \times t_T} \quad (10)$$

Based on numerous HiL simulations, it is seen that  $E_L$  of the 1 MW GCPVS is at most 86.58 Wh. By considering  $t_T = 2$  s and  $P_{MPP} = 1$  MW, the generated energy during  $t_T$  without disturbance injection, is 555.55 Wh; hence, the relative energy loss is 15.58% and GCPVS efficiency is 84.42%. Moreover, the total energy loss in a given time interval relies on the number of disturbance injection. A higher number of

disturbance activation results in a greater loss and lower efficiency. Fig. 17 displays the efficiency descent of the 1 MW GCPVS based upon the number of disturbance injection in one hour. For instance, if the employed disturbance is triggered once a minute (the disturbance is switched off for 29 number of 2 s time frames and activates for one), the efficiency lessens by 0.519%. Hence, the influence of the proposed scheme on GCPVS efficiency is hardly noticeable.

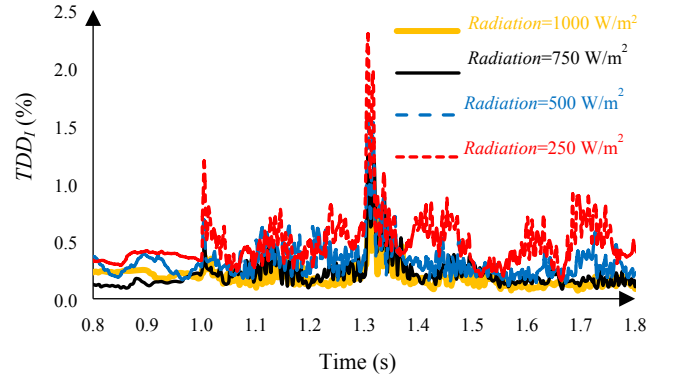


Fig. 14. Total demand distortion of the output current during disturbance insertion.

## 5. Comparison and discussions

### 5.1. Comparison with existing algorithms

The proposed method has been compared with several IDMs in the standpoints of NDZ, detection time, the burden of the required data, threshold dependency on the studied network, level of cost and complexity, and level of efficiency and PQ drops, summarized in Table 3.

- As described earlier, the NDZ of the proposed MPPT-based technique includes an eminently small range of active power mismatches, e.g.  $\pm 1\%$  for  $V_T = 0.5\%$ , implying outstanding performance in a wide range of critical scenarios.
- In the presented methodology, the first level distinguishes suspicious islanding events through comparing absolute voltage deviation ( $|\Delta V_{PCC}|$ ) with  $V_T$  within two operating cycles. Afterward, the disturbance is injected into the PV array reference voltage to decline the PCC voltage. Based on the presented HiL simulations, the output voltage goes below the UV relay set in at most 100 ms. Therefore, the maximum islanding detection time of the presented technique is 137 ms, which is among the fastest existing algorithms.
- In the provided technique, the  $|\Delta V_{PCC}|$  should be defined in each cycle and a disturbance is then involved into  $V_{PV,ref}$  under  $|\Delta V_{PCC}| \geq V_T$ . The PCC voltage is retrieved in the detection process and therefore, the computation burden of the presented IDM is low, similar to the conventional passive and active IDMs. Conversely, the training and classification of the mathematical-based passive criteria require a large data of the local variables [13–17].
- The new passive IDMs are reported with reliable performance even in low power mismatch scenarios [8–10]. Nevertheless, the methods threshold(s) are heavily depended on the case study system. Although the mathematical tools are also proven to be accurate islanding classifiers [13–17], the settings are defined through extensive islanding and non-islanding tests, i.e. time-consuming simulations should be repeated for a new DG/network. On contrary, the thresholds of the proposed two-level IDM are established analytically irrespective of the studied network.
- In the frequency-based IDMs such as AFD and SFS, the disturbance has been applied to the frequency of the DG current, enlarging its harmonics [18,19]. The harmonic current has been also perturbed in impedance measurement to discriminate islanding through PCC impedance at the corresponding harmonic [20]. Therefore, the PQ has been degraded moderately in these IDMs. However, the PQ of the GCPVS, equipped with the recommended technique has been met in all conditions as unveiled in the presented analyses.
- VPF-based IDMs are known as simple and strong islanding classifiers with small NDZ [21–24]. These schemes have been designed in a way that the magnitude of the current fundamental frequency would be

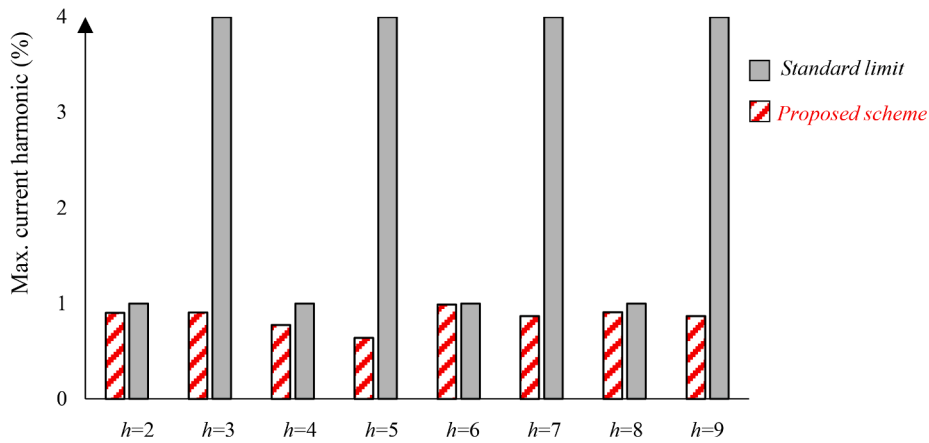


Fig. 15. Harmonic spectra of the GCPVS output current during disturbance injection.

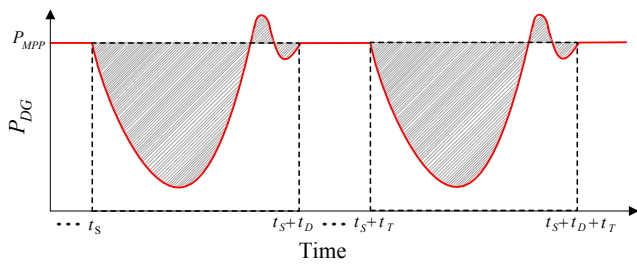


Fig. 16. DG active power output during injection of the proposed disturbance.

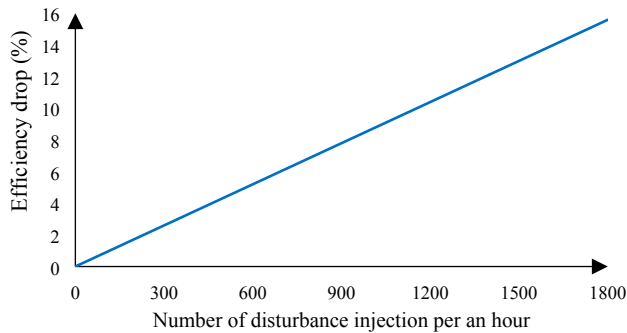


Fig. 17. Effect of disturbance injection number on the GCPVS efficiency.

changed during the disturbance insertion. This selection results in a successful shift of PCC voltage out of standard range; however, the real power output has been lowered significantly during non-islanding switching events with great PCC voltage variation. Conversely, the efficiency drop for the presented two-level methodology is limited, irrespective of the size of output voltage variation.

5.2. Discussions

This part discusses the assumptions, results of the presented HiL simulations, and future studies to enhance the effectiveness of the proposed methodology.

- In addition to the PCC voltage deviation ( $|\Delta V_{PCC}| \geq V_T$ ), the presented MPPT based-disturbance can be triggered through a frequency index in the first level. This mitigates the NDZ effectively in the term of relative reactive power mismatches as shown in Fig. 18.
- The basic idea of the proposed algorithm is to deviate the PV operating point from MPP for reducing the active power output and consequently the PCC voltage in islanded mode. In all presented scenarios, the uniform received radiation and MPP performance of the PV array before disturbance injection are hypothesized. During the non-uniform radiation situation, two cases can be considered for PV operating point before disturbance insertion: a) global MPP (GMPP) performance, reached by several mathematical-based algorithms such as meta-heuristic [34,35], and b) local MPP (LMPP) performance, i.e. conventional searched-based technique fails to find the global one. In the latter scenario, the disturbance injection in  $V_{PV,ref}$  may change the active power output in both manners as illustrated in Fig. 19. Therefore, the PCC voltage may rise or fall moderately

Table 3 Comparison of the recommended algorithm with several existing active IDMs.

Methodology	NDZ ( $\Delta P/P_{DG}$ )	Detection time	Data burden	Settings dependency	Cost and complexity	PQ degradation	Efficiency drop
Rate of change of equivalent resistance at PCC [8]	Near zero	60 ms	Medium	High	Low	Low	Low
Rate of change of reactive power [9]	Near zero	100 ms	Low	High	Low	Low	Low
Support vector machine [16,17]	Zero	60 ms	High	High	High	Low	Low
AFD [18]	Medium	2 s	Low	Medium	Medium	High	Low
SFS [19]	Small	2 s	Low	Medium	Medium	High	Low
Impedance measurement [20]	Near zero	200 ms	Low	High	High	High	Low
VPF [21]	Large	500 ms	Low	Medium	Low	Medium	Medium
Voltage negative feedback [22]	Zero	900 ms	Low	Medium	Low	Medium	Medium
Improved VPF [23]	Near zero	300 ms	Low	Medium	Low	High	Medium
Modified sliding mode [24]	Zero	250 ms	Low	Medium	Medium	Medium	Medium
d-axis equivalent resistance [25]	Zero	800 ms	Low	High	High	Medium	Low
Parallel impedance switching [26]	Zero	300 ms	Medium	High	High	Low	Low
Two-level MPPT-based algorithm	Near zero	137 ms	Low	Low	Low	Low	Low

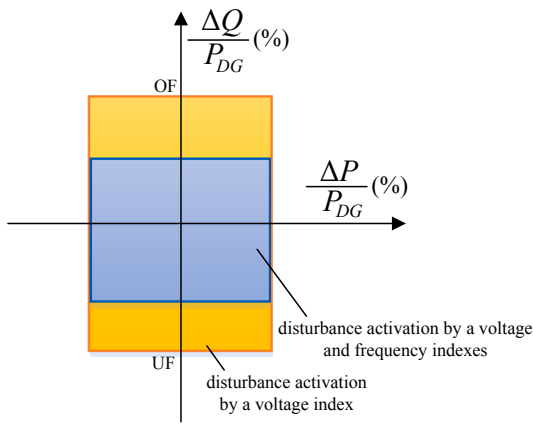


Fig. 18. NDZ mitigation of the presented technique in term of relative active power mismatch.

without leaving the standard range. Moreover, although the generated active power reduces after involving the presented disturbance in the GMPP state,  $P_{DIS}$  may be insufficient ( $P_{DIS}/P_{DG} < 56.25\%$ ) to decline the PCC voltage below the UV relay set (Fig. 19). Summarily, the PV array power reduction in partial shading cases may not decrease the PCC voltage notably, and islanding remains undetected after disturbance injection. A further study is hence necessary to ensure the reliable performance in such conditions.

- As explained earlier, the NDZ of the presented technique includes a narrow range of active power mismatches. In order to eliminate the NDZ, a small disturbance can be injected periodically to the  $V_{pv,ref}$  to decrease the active power output slightly (Fig. 20). In the islanding mode, this small  $P_{DG}$  drop leads to the active power mismatch with  $|\Delta V_{PCC}|$  greater than  $V_T$ , even in the fully-balanced island. The main disturbance is triggered accordingly to drift the voltage below the UV set. The frequency and size of this periodic disturbance should be selected precisely to minimize the detection time and efficiency drop as well as ensuring the islanding classification in all case studies.

6. Conclusions

This paper deals with a new high power quality two-level maximum power point tracking-based islanding detection method for grid-connected photovoltaic system-based microgrid. In the first level of the recommended technique, the absolute voltage deviation is exploited to recognize the suspicious islanding states. Afterward, a disturbance is injected into the MPPT algorithm to diminish the active power output and PCC voltage considerably. According to the outputs of various hardware-in-the-loop tests, this disturbance shifts the PCC voltage beyond the minimum standard set for islanding classification within 137 ms except for a narrow  $\pm 1\%$  range of relative active power mismatches. The automatic MPP restoration also boosts the chance of maximum active power generation in the standalone microgrid after 500 ms of islanding recognition. From the power quality standpoint, it is demonstrated that unlike the conventional active IDMs, the total demand distortion of the output current augments slightly during the disturbance injection. The harmonic components of the output current are also increased, e.g. 0.989% for the 6th harmonic as the greatest one; nevertheless, they do not violate the standard limits.

It has been finally shown that the presented two-level MPPT-based technique not only timely and accurately categorizes the islanding operating mode, but its impact on the power quality degradation is also negligible. Therefore, it can be developed to the existing voltage source inverters as a strong islanding classifier.

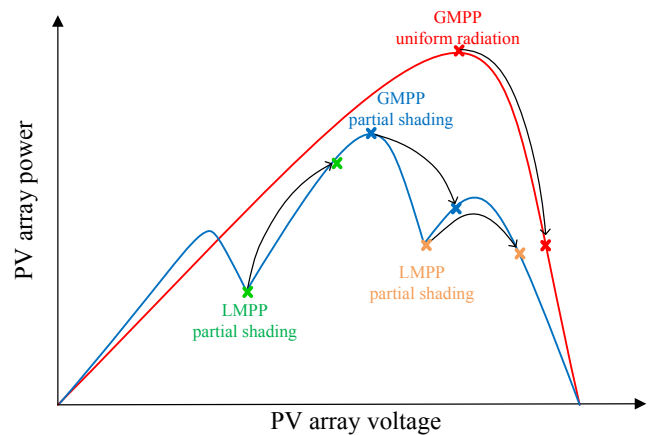


Fig. 19. Performance of the proposed algorithm in partial shading situation.

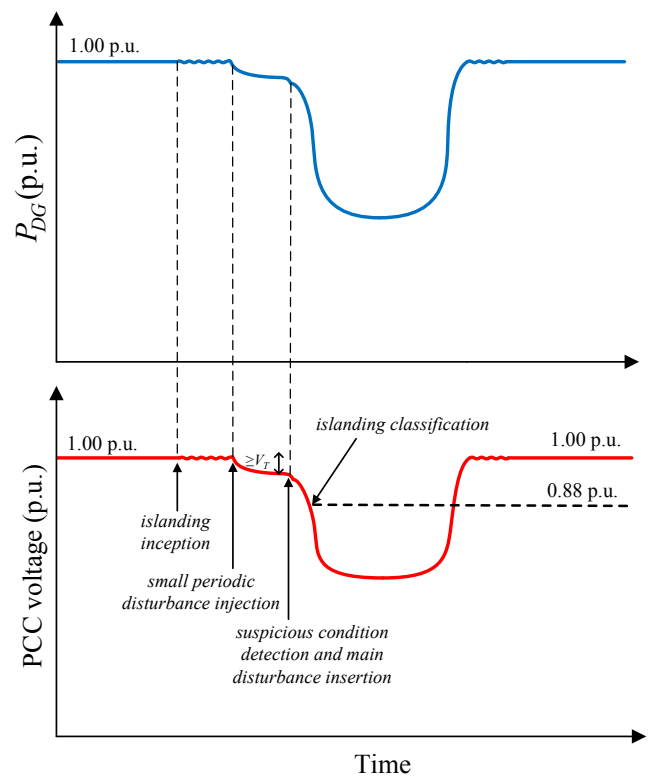


Fig. 20. Small periodic disturbance injection to eliminate the NDZ.

Declaration of Competing Interest

The authors declare that they have no known competing financial interests or personal relationships that could have appeared to influence the work reported in this paper.

References

- [1] Shafique M, Luo X, Zuo J. Photovoltaic-green roofs: A review of benefits, limitations, and trends. *Sol Energy* 2020;202:485–97.
- [2] Kim M-S, Haider R, Cho G-J, Kim C-H, Won C-Y, Chai J-S. Comprehensive review of islanding detection methods for distributed generation systems. *Energies* 2019;12 (5):837.
- [3] Mishra M, Chandak S, Rout PK. Taxonomy of islanding detection techniques for distributed generation in microgrid. *Renewable Energy Focus* 2019;31:9–30.
- [4] Characteristics of the utility interface for photovoltaic (PV) systems. IEC 61727, 2002.
- [5] IEEE Standard 1547–2003, 2003..

- [6] Poluektov A, Pinomaa A, Romanenko A, Ahola J, Kosonen A. Sensitivity analysis of a PLC-based DSSS anti-islanding system in power distribution grids. *Int J Electr Power Energy Syst* 2019;113:739–47.
- [7] Bayrak G, Kabalci E. Implementation of a new remote islanding detection method for wind–solar hybrid power plants. *Renew Sustain Energy Rev* 2016;58:1–15.
- [8] Xie X, Huang C, Li D. A new passive islanding detection approach considering the dynamic behavior of load in microgrid. *Int J Electr Power Energy Syst* 2020;117:105619.
- [9] Nikolovski S, Baghaee HR, Mlakić D. Islanding detection of synchronous generator-based DGs using rate of change of reactive power. *IEEE Syst J* 2019;13(4):4344–54.
- [10] Grebla M, Yellajosula JRAK, Hoidalén HK. Adaptive frequency estimation method for ROCOF islanding detection relay. *IEEE Trans on Power Delivery* 2020;35(4):1867–75.
- [11] Ostojic MM, Djuric MB. The algorithm with synchronized voltage inputs for islanding detection of synchronous generators. *Int J Electr Power Energy Syst* 2018;103:431–9.
- [12] Abd-Elkader AG, Saleh SM, Magdi Eiteba MB. A passive islanding detection strategy for multi-distributed generations. *Int J Electr Power Energy Syst* 2018;99:146–55.
- [13] Mlakić D, Baghaee HR, Nikolovski S. A novel ANFIS-based islanding detection for inverter-interfaced microgrids. *IEEE Trans on Smart Grid* 2019;10(4):4411–24.
- [14] Ahmadipour M, Hizam H, Lutfi Othman M, Radzi MAM, Chireh N. A novel islanding detection technique using modified Slantlet transform in multi-distributed generation. *Int J Electr Power Energy Syst* 2019;112:460–75.
- [15] Pinto SJ, Panda G. Performance evaluation of WPT based islanding detection for grid-connected PV systems. *Int J Electr Power Energy Syst* 2016;78:537–46.
- [16] Baghaee HR, Mlakić D, Nikolovski S, Dragicevic T. Anti-islanding protection of PV-based microgrids consisting of PHEVs using SVMs. *IEEE Trans on Smart Grid* 2020;11(1):483–500.
- [17] Baghaee HR, Mlakić D, Nikolovski S, Dragicević T. Support vector machine-based islanding and grid fault detection in active distribution networks. *IEEE Journal of Emerging and Selected Topics in Power Electronics* 2020;8(3):2385–403.
- [18] Lopes LAC, Sun H. Performance assessment of active frequency drifting islanding detection methods. *IEEE Trans on Energy Conversion* 2006;21(1):171–80.
- [19] Yafaoui A, Wu B, Kouro S. Improved active frequency drift anti-islanding detection method for grid connected photovoltaic systems. *IEEE Trans on Power Electronics* 2012;27(5):2367–75.
- [20] Reigosa D, Briz F, Blanco C, García P, Guerrero JM. Active islanding detection using high-frequency signal injection. *IEEE Trans on Industry Applications* 2012;48(5):1588–97.
- [21] Samui A, Samantaray SR. An active islanding detection scheme for inverter-based DG with frequency dependent ZIP-exponential static load model. *Int J Electr Power Energy Syst* 2016;78:41–50.
- [22] Bakhshi-Jafarabadi R, Sadeh J. New voltage feedback-based islanding detection method for grid-connected photovoltaic systems of microgrid with zero non-detection zone. *IET Renew Power Gener* 2020;14(10):1710–9.
- [23] Bei T-Z. Accurate active islanding detection method for grid-tied inverters in distributed generation. *IET Renew Power Gener* 2017;11(13):1633–9.
- [24] Bakhshi R, Sadeh J. Voltage positive feedback based active method for islanding detection of photovoltaic system with string inverter using sliding mode controller. *Sol Energy* 2016;137:564–77.
- [25] Sivadas D, Vasudevan K. An active islanding detection strategy with zero non-detection zone for operation in single and multiple inverter mode using GPS synchronized pattern. *IEEE Trans on Industrial Electronics* 2020;67(7):5554–64.
- [26] Rostami A, Jalilian A, Zabihi S, Olamaei J, Poursmaeil E. Islanding detection of distributed generation based on parallel inductive impedance switching. *IEEE Syst J* 2020;14(1):813–23.
- [27] Khodaparastan M, Vahedi H, Khazaeli F, Oraee H. A novel hybrid islanding detection method for inverter-based DGs using SFS and ROCOF. *IEEE Trans on Power Delivery* 2017;32(5):2162–70.
- [28] R. Zamani, MEH. Golshan, HH. Alhelou, N. Hatziargyriou. A novel hybrid islanding detection method using dynamic characteristics of synchronous generator and signal processing technique. *Electric Power Systems Research* 2019;175:105911.
- [29] M. Hamzeh, H. Mokhtari. Power quality comparison of active islanding detection methods in a single phase PV grid connected inverter. 2009 IEEE International Symposium on Industrial Electronics, Seoul, South Korea, 2009.
- [30] IEEE recommended practice for utility interface of photovoltaic (PV) systems. *IEEE Standard 929–2000*, 2000.
- [31] Hassaine L, Olias E, Quintero J, Salas V. Overview of power inverter topologies and control structures for grid connected photovoltaic systems. *Renew Sustain Energy Rev* 2014;30:796–807.
- [32] Yang B, Zhu T, Wang J, Shu H, Yu T, Zhang X, et al. Comprehensive overview of maximum power point tracking algorithms of PV systems under partial shading condition. *J Cleaner Prod* 2020;268:121983.
- [33] Wen Yin O, Chitti Babu B. Simple and easy approach for mathematical analysis of photovoltaic (PV) module under normal and partial shading conditions. *Optik* 2018;169:48–61.
- [34] Yang B, Zhong L, Zhang X, Shu H, Yu T, Li H, et al. Novel bio-inspired memetic salp swarm algorithm and application to MPPT for PV systems considering partial shading condition. *J Cleaner Prod* 2019;215:1203–22.
- [35] Yang B, Yu T, Zhang X, Li H, Shu H, Sang Y, et al. Dynamic leader based collective intelligence for maximum power point tracking of PV systems affected by partial shading condition. *Energy Convers Manage* 2019;179:286–303.